J. Fluid Mech. (1994), *vol.* 278, *pp.* 267–287

The viscosity of bimodal and polydisperse suspensions of hard spheres in the dilute limit

By N. J. WAGNER[1]† AND A. T. J. M WOUTERSEN[2]‡

[1]Department of Chemical Engineering, University of Delaware, Newark DE 19716 USA

[2]The University of Utrecht, Department of Physical and Colloid Chemistry, Utrecht, Netherlands

(Received 22 November 1993 and in revised form 25 May 1994)

An exact result is calculated numerically for the dilute limiting, zero shear viscosity of bimodal suspensions of hard spheres. The required hydrodynamic functions are calculated from recent results for the resistivities of unequal spheres. Both the hydrodynamic and Brownian contributions to the Huggins coefficient exhibit a minimum that is symmetric in mixing volume fraction. The resultant minimum deepens with increasing size ratio. The results are discussed in the light of published measurements of the viscosity for bimodal suspensions and previous phenomenological theories. The reduction of viscosity upon mixing is seen to be a result of near-field hydrodynamic shielding of asymmetric particle pairs. It is also shown that the use of far-field hydrodynamic interactions yields qualitatively incorrect results for the viscosity of binary mixtures. A parametrization of the bimodal results allows an estimation of the effects of suspension polydispersity on the Huggins coefficient. For polydispersities of ten percent or less, the Huggins coefficient is essentially unchanged from the value calculated for an equivalent, monodisperse suspension at equal volume fraction. A parametrization of these results is provided for relating the reduction in Huggins coefficient to the polydispersity index.

1. Introduction

The importance of polydispersity on the equilibrium and mechanical properties of colloidal suspensions has been a significant technological and scientific issue (Sweeny & Geckler 1954; Chong, Christiansen & Baer 1971; Jeffrey & Acrivos 1976; Dickinson, Parker & Lal 1981; Stapleton, Tildesley & Quirke 1990; D'Aguanno & Klein 1991; D'Aguanno *et al.* 1993; Woutersen 1992). Indeed, technologies have employed mixing of specific size ratios to achieve flowability at high solids concentrations (Chong *et al.* 1971; Goto & Kuno 1984; Senqun & Probstein 1989; Shapiro & Probstein 1992). It is almost universally observed that the addition of a small volume of particles of small size to an already concentrated suspension of big particles results in dramatic viscosity reductions (Sweeny & Geckler 1954; Chong *et al.* 1971; Goto & Kuno 1982, 1984). Further, at fixed total volume fraction, the viscosity of a bimodal suspension usually shows a minimum with respect to mixing volume ratio of the two sizes, and this minimum is on the side rich in large particles (Farris 1968; Ackermann & Shen 1979; Goto & Kuno 1984).

† To whom correspondence should be sent.

‡ Current address: DSM Research, 6160 MD, Geleen, The Netherlands.

Phenomenological theories have been developed to explain the viscosity reductions that can arise from mixing particles of different mean size distributions (Farris 1968; Chong *et al.* 1971). Most of these references deal with relatively large particles such that Brownian motion does not directly influence the rheology. The proposed mechanism is based on an excluded volume effect (Ackermann & Shen 1979; Goto & Kuno 1984; Shapiro & Probstein 1992), where size asymmetry results in a more efficient packing and a higher total solids volume fraction. Often in modelling suspensions with large size asymmetries, the small particles are taken to act as a filler for an effective fluid within which the large particles move (Roscoe 1952; Senqun & Probstein 1989). We are aware of only two previous attempts to use particle microhydrodynamics and statistical mechanics to rigorously calculate this mixing effect (Ohtsuki 1983; van Iersel 1987), wherein the major impediment was the lack of hydrodynamic interaction coefficients for unequal spheres. Recent Stokesian dynamics simulations by Chang & Powell (1993) of hard spheres in two dimensions have qualitatively demonstrated some of the aforementioned experimental observations. Clearly, an exact calculation of bimodal suspension viscosity could provide important physical insight and a firm foundation for understanding this viscosity reduction effect. Given our ignorance concerning many-body interactions in suspensions, such an exact calculation is only feasible for the dilute, or two-body limit. Exact calculations for the effects of polydispersity on the sedimentation velocity and diffusivity for dilute suspensions of colloidal particles have been performed (Batchelor & Wen 1982*a*, *b*; Batchelor 1983). However, to date there have been no exact calculations of the influence of polydispersity on the shear viscosity and only recently have there been attempts to measure this phenomenon for low concentrations of particles by Woutersen & de Kruif (1993), and for higher concentrations by Rodriguez, Kaler & Wolfe (1992). As calculations at high Péclet number, which would more closely correspond to the bulk of the experimental data mentioned above, are not feasible for shear flows (see Batchelor & Green 1972*a*, *b*), a logical starting place is the tractable regime of low Péclet number.

Such a calculation has additional value as the dilute limiting viscosity is an important physical characterization measurement for colloid scientists. Expanding the ratio of suspension to solvent viscosity (μ_o) in terms of powers of particle mass concentration c yields a virial expansion:

$$\eta_s/\mu_o = 1 + [\eta]_o c + k_H [\eta]_o^2 c^2 + \ldots, \tag{1.1}$$

where $[\eta]_o$ is the intrinsic viscosity, which is related to the molecular weight or volume of the particle (Hiemenz 1986), and k_H is the Huggins coefficient. Determination of the Huggins coefficient yields important information about the colloidal forces (Russel 1984; Russel, Saville & Schowalter 1989). This is analogous to measuring the second virial coefficient for the pressure, which can be written purely in terms of the interparticle force law (McQuarrie 1976). Thus, exact calculations of the Huggins coefficient are necessary for extracting the interparticle potential from viscosity measurements. As will be shown, the Huggins coefficient also depends explicitly upon the size ratio of the particles and, hence, polydispersity. Thus, confident use of this experimental technique requires knowing how the Huggins coefficient varies with size polydispersity.

Recently, Jeffrey (1992) has calculated the hydrodynamic resistivities between pairs of hard, spherical particles of different radii. As shown here, this becomes the basis for the exact numerical calculation of the limiting viscosity of dilute, bimodal suspensions of hard spheres. In what follows, we employ the established derivations

of Batchelor & Green (1972), and Batchelor (1976) to determine the stresses acting in a bimodal suspension of hard spheres in the dilute limit. Both the stresses and the radial distribution function are calculated numerically in the linear response limit. Results are obtained for the limiting viscosity of bimodal mixtures up to size ratios of 10 as a function of the relative volume ratio. This becomes the basis for calculating the limiting viscosity of dilute suspensions with arbitrary size distribution. Results are then presented for a continuous Schulz distribution of sizes as a function of polydispersity.

2. Stresses

The effective suspension viscosity η_s, which is a complex quantity for viscoelastic materials, is defined for steady shear as

$$\boldsymbol{\Sigma} = I.T. + 2\eta_s ptptpt\boldsymbol{E} = I.T. + 2\mu_o \boldsymbol{E} + \langle \boldsymbol{S}^I \rangle + \langle \boldsymbol{S}^B \rangle + \langle \boldsymbol{S}^H \rangle, \tag{2.1}$$

where $\boldsymbol{\Sigma}$ denotes the stress tensor and $I.T.$ is an isotropic term not of interest here. The second term on the right-hand side is the solvent contribution (μ_o being the solvent viscosity). The following terms are the explicit contributions from interparticle forces (^{I}), Brownian motion (^{B}), and hydrodynamic interaction (^{H}), separated out as stresslets. The brackets $\langle\ \rangle$ denote an ensemble average over all N particles in volume V, which are subjected to an applied flow field characterized by the rate of strain tensor $\boldsymbol{E}$.

The stresslets arising from the various colloidal forces are calculated by ensemble averaging the appropriate pair stresslet over the pair distribution function characterizing the suspension microstructure. For the low shear viscosity only the equilibrium and linear response microstructures are necessary to calculate the stresslets to linear order in the strain rate. Because the necessary equations relating these stresslets to the interparticle forces have been previously derived by Batchelor & Green (1972*a*, *b*), Batchelor (1977) and Felderhof & Jones (1987) and are frequently used for calculation of the viscosity (see, for example Russel 1984; Wagner & Russel 1989; Dhont 1989; Brady & Bossis 1988; Brady 1993*a*, *b*), only an overview of the derivation will be presented here. The interested reader is encouraged to examine the works of Batchelor & Green (1972*a*, *b*) and Batchelor (1977) for the complete derivations.

The hydrodynamic contribution to the stresses arises because the solid particles do not deform with the surrounding fluid, but rather, generate additional strain fields in the flowing fluid. As these fields influence other Brownian particles and propagate over long range, rigorous accounting of the total hydrodynamic stress is a non-trivial problem requiring renormalization (Batchelor & Green 1972*a*, *b*; Batchelor 1977; Felderhof 1988). Rigorous results are possible in the limit of pair hydrodynamic interactions for the stress dipoles. Batchelor & Green (1972*a*, *b*) summed over these dipoles to calculate their contribution to the bulk stress.

$$\left.\begin{aligned} \langle \boldsymbol{S}^H \rangle &= 2\boldsymbol{E}\mu_o \left(\tfrac{5}{2}\phi + \tfrac{5}{2}\phi^2 + \frac{\phi^2}{v^2}\left(\frac{4\pi}{3}\right)^2 \int\int a^3 \rho(a)\mathrm{d}a\, b^3 \rho(b)\mathrm{d}b\, I^H\left(\frac{b}{a}\right)\right), \\ I^H\left(\frac{b}{a}\right) &= \frac{15}{2b^3}\int_{a+b}^{\infty} \hat{J}\left(\frac{r}{a}, \frac{b}{a}\right) g\left(\frac{r}{a}, \frac{b}{a}\right) r^2 \mathrm{d}r, \\ v &= \frac{\phi}{n} = \int_0^{\infty} \frac{4\pi}{3} a^3 \rho(a)\mathrm{d}a. \end{aligned}\right\} \tag{2.2}$$

The first term $\frac{5}{2}\phi$, (with $\phi = \frac{4}{3}\pi a^3 n$ the particle volume fraction where n is the number density) is the classical Einstein contribution, which is calculated by integrating over the disturbance flow field due to a single particle. The $\frac{5}{2}\phi^2$ term arises from renormalizing the summation over hydrodynamic dipoles, which leads to the integral, written in convergent form above. Note the additional dependence on volume fraction through the pair correlation function $g(r/a,\ b/a)$. The hydrodynamic function $\hat{J}(r/a,\ b/a)$ characterizes the stresslet induced on a particle pair by the applied shear. Notice also that to linear order in the shear rate this stress depends only on the equilibrium structure. This is intuitive as the hydrodynamic dipoles are themselves induced by the flow; thus this source of additional stress is already of linear order in the deformation.

For bidisperse systems the equations become

$$\langle \boldsymbol{S}^H \rangle = 2\mu_o \boldsymbol{E} \left(\frac{5}{2}\phi + \frac{5}{2}\phi^2 + \sum_{i,j=1}^{2} \phi_i \phi_j I^H(\lambda_{ij}) \right), \tag{2.3}$$

with $\lambda_{ij} = a_i/a_j$ the size ratio.

The contribution from the thermodynamic forces to the stresslet has two parts: the direct interaction of particles, and the induced hydrodynamic stresslets due to these forces inducing particle motion. It is well established that the lubrication forces, which prevent interparticle interpenetration, also nullify any contribution from the hard-sphere potential (Brady & Bossis 1988; Wagner & Russel 1989). Thus, only the Brownian motion contributes to the thermodynamic stresslets for hard spheres. The presence of hydrodynamic interaction couples the relative Brownian motion of two particles in the suspension (Batchelor 1976,1977; Brady & Bossis 1988; Brady 1993*a*, *b*). For example, two particles close together at some instant in time experience a correlated Brownian force due to the intervening solvent that prevents the stochastic Brownian forces from overlapping two hard particles. Calculation of the stress requires renormalization as the integral over these stresslets is non-convergent due to the long ranges of the non-equilibrium structure and the hydrodynamic coupling. The result of this operation as performed by Batchelor (1977) is a convergent expression for the Brownian stress, which in the two-particle limit becomes

$$\left.\begin{aligned} \langle \boldsymbol{S}^B \rangle &= -\frac{1}{2} kT \int W(r) \left(\frac{\boldsymbol{rr}}{r^2} - \tfrac{1}{3}\boldsymbol{I} \right) P_2(\boldsymbol{r}) \mathrm{d}\boldsymbol{r}, \\ W(r) \left(\frac{\boldsymbol{rr}}{r^2} - \tfrac{1}{3}\boldsymbol{I} \right) &= 2\nabla \cdot \boldsymbol{C}; \end{aligned}\right\} \tag{2.4}$$

with $\boldsymbol{C}$ the shear mobility tensor defined as:

$$C_{\alpha\beta\gamma}(r) = -(A(r) - B(r)) \frac{r_\alpha r_\alpha r_\alpha}{2r^2} + \tfrac{1}{6} A(r) r_\gamma \delta_{\alpha\beta} - \tfrac{1}{4} B(r)(r_\alpha \delta_{\beta\gamma} + r_\beta \delta_{\alpha\gamma}). \tag{2.5}$$

Here the scalar functions $A(r)$ and $B(r)$ are calculated for specific size ratios (see Appendix A).

The non-equilibrium pair distribution function $P_2(\boldsymbol{r})$ can be calculated in the linear response limit. The angular dependence can be separated out along with the equilibrium structure to yield

$$P_2\left(\boldsymbol{r}, \frac{b}{a}\right) = n^2 g\left(\frac{r}{a}, \frac{b}{a}\right) \left(1 - Pe\, \frac{\boldsymbol{rr}}{r^2} : \hat{\boldsymbol{E}} f\left(\frac{r}{a}, \frac{b}{a}\right)\right). \tag{2.6}$$

The function $f(r/a, b/a)$ is the radial component of the shear distortion and the Péclet number, defined as

$$Pe = \frac{3\pi\mu_0(a+b)ab \mid \boldsymbol{E} \mid}{2k_bT}, \tag{2.7}$$

gauges the relative strength of the flow to the Brownian motion. Using the above the Brownian stress for a polydisperse suspension in the two-body limit and written explicitly in terms of a continuous size distribution becomes

$$\langle \boldsymbol{S}^B \rangle = kT\frac{n^2}{2}\int\int\int \rho(a)\mathrm{d}a\rho(b)\mathrm{d}bW_{ab}\left(s,\frac{b}{a}\right)\left(\frac{\boldsymbol{ss}}{s^2}-\frac{1}{3}\boldsymbol{I}\right) Pe\left(\frac{b}{a}\right)g\left(s,\frac{b}{a}\right)f\left(s,\frac{b}{a}\right)\left(\frac{\boldsymbol{ss}}{s^2}\right)\mathrm{d}\,s:\hat{\boldsymbol{E}} \tag{2.8}$$

where $s = 2r/(a+b)$.

Substitution of the bimodal size distribution,

$$\rho(a) = x_1\delta(a-a_1) + x_2\delta(a-a_2) \tag{2.9}$$

with x_i the number fraction of type i, and integration over the angular terms yields

$$\langle \boldsymbol{S}^B \rangle = 2\mu_o\boldsymbol{E}\sum_{i,j=1}^{2}\phi_i\phi_j I^B(\lambda_{ij}). \tag{2.10}$$

Here,

$$\left.\begin{aligned} I^B(\lambda_{ij}) &= \tfrac{9}{40}\left(\tfrac{1}{2}(1+\lambda_{ij})\right)^4\lambda_{ij}^{-2}\int_2^\infty s^2 g_{ij}(s,\lambda_{ij})f_{ij}(s,\lambda_{ij})W_{ij}(s,\lambda_{ij})\mathrm{d}s, \\ s &= \frac{2r_{ij}}{a_i+a_j}. \end{aligned}\right\} \tag{2.11}$$

It is clear from the above equations that calculation of the hydrodynamic contribution can proceed given an expression for the equilibrium pair distribution function and the bimodal hydrodynamic coefficients. However, the Brownian contribution requires explicit knowledge of the linear response term for the pair distribution function under an applied shear field. Earlier work by Batchelor & Green (1972) provides a method for calculating this distortion using a Smoluchowski equation for the dynamics.

3. Smoluchowski equation for the non-equilibrium structure

The non-equilibrium microstructure of colloidal dispersions can be directly calculated from a Smoluchowski equation (Batchelor & Green 1972*a*, *b*; Batchelor 1977; Ohtsuki 1981; Felderhof 1988). This N-body conservation equation in configuration space is the continuity equation for the N-body probability P_N with the flux given by the linear relationship $P_N\boldsymbol{U}_i$ with $\boldsymbol{U}_i$ the velocity of the ith particle. The conservation equation in configuration space is integrated directly to the pair level, neglecting all higher-order correlations, to yield

$$\frac{\partial P_2}{\partial t} + \nabla\cdot(P_2\boldsymbol{U}) = 0, \tag{3.1}$$

defining the relative velocity $\boldsymbol{U} = \boldsymbol{U}_2 - \boldsymbol{U}_1$, which is obtained from a colloidal force balance containing the details of the interactions between two particles. At the two-body level this force balance becomes

$$-k_bT\nabla \ln P_2 + \nabla \boldsymbol{\Phi} = \boldsymbol{D}^{-1} \cdot (\boldsymbol{U} - \boldsymbol{\Gamma} \cdot \boldsymbol{s} + 2\boldsymbol{C} : \boldsymbol{E}),$$
$$\boldsymbol{\Gamma} \cdot \boldsymbol{s} = \boldsymbol{E} \cdot \boldsymbol{s} + \boldsymbol{\Omega} \times \boldsymbol{s} \tag{3.2}$$

The first term is the Brownian or entropic force, given as the gradient of the probability distribution (Batchelor 1976) while the second is the interparticle force, written in terms of the pair potential $\boldsymbol{\Phi}$. Balancing these is the hydrodynamic force, where $\boldsymbol{D}$ denotes the relative Brownian diffusivity

$$\boldsymbol{D}(s^N)/D_0 = G\left(s, \frac{b}{a}\right)\frac{\boldsymbol{ss}}{s^2} + H\left(s, \frac{b}{a}\right)\left(\boldsymbol{I} - \frac{\boldsymbol{ss}}{s^2}\right), \quad D_0 = \frac{k_bT}{3\pi\mu_0(a+b)/2}, \tag{3.3}$$

with G and H scalar functions of the configuration, and $\boldsymbol{C}$ the shear mobility tensor defined above.

We further limit the calculation to steady, weak flows. Substitution into the force balance (3.2) and integration with the flux equation (3.1) yields the microstructure equation for the unknown function $f(s)$ to linear order in Pe as

$$\frac{1}{g(s)s^2}\frac{\mathrm{d}}{\mathrm{d}s}\left(g(s)s^2G(s)\frac{\mathrm{d}f(s)}{\mathrm{d}s}\right) - 6H(s)\frac{f(s)}{s^2} = -W(s) - s(1 - A(s))\frac{\mathrm{dln}g(s)}{\mathrm{d}s}, \tag{3.4}$$

where it is understood that the functions $g(s)$, $f(s)$, $G(s)$, $H(s)$, and $W(s)$ are functions of the size ratio λ and the subscripts for particle type $(_{ij})$ have been omitted for clarity. Note that $g(s)$ becomes a simple step function in the two-particle limit (Batchelor 1977).

Arguments by Dhont (1987) show that the structure induced by shear distortion is a non-analytic function of the shear rate such that the ansatz of linear response is not strictly valid. Qualitatively the argument can be demonstrated by examining the two-particle Smoluchowski equation, (3.1) and (3.2). The second term on the right-hand side of (3.2) describes the flow distortion. Even for small shear rates this distortion can be arbitrarily large as $s \to \infty$. However, the linear response ansatz requires this shear perturbation to always be small relative to the leading-order terms. As shown by Dhont, this leads to boundary-layer behaviour at large values of s. Fortunately, in the limit of zero shear the effects of this boundary layer can be shown to be inconsequential and, rigorously, the linear response term is the valid solution. Although the non-analyticity does not affect the work presented here, we caution that it does require consideration when solving the Smoluchowski equation for finite shear rates.

4. Results and discussion

4.1. *Bimodal suspensions*

Direct calculation of the functions I^H and I^B require hydrodynamic mobilities for unequal spheres. These were calculated from Jeffrey's resistivities, as shown in Appendix A. For the Brownian component, the calculation of the non-equilibrium structure factor was performed numerically by matrix inversion of the discretized version of the linearized Smoluchowski equation. A numerical algorithm (Press *et al.* 1986) was employed for direct inversion of the resultant tridiagonal matrix of coefficients. All the hydrodynamic coefficients were interpolated from spline fits of the

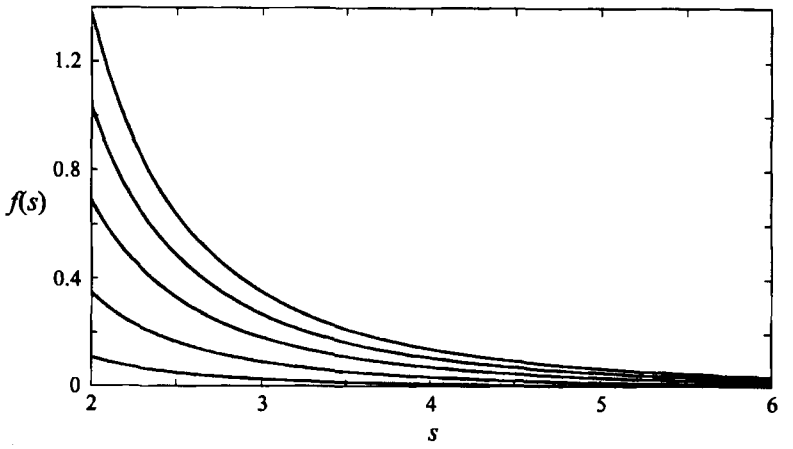

FIGURE 1. The non-equilibrium structure function $f(s)$ plotted for various degrees of size asymmetry, λ= 1, 2, 3, 5, 10 top to bottom, respectively.

λ	$I^B(\lambda)$	$I^H(\lambda)$
1.0	0.950	2.50
1.25	0.913	2.48
1.6	0.848	2.42
2.0	0.742	2.34
4.0	0.384	2.05
5.0	0.297	1.98
6.4	0.207	1.92
8.0	0.150	1.89
10	0.105	1.86

TABLE 1. Bimodal I^B and I^H Functions

coefficients calculated at discrete intervals. All calculations were converged to results independent of mesh size and the interval over which the coefficients were calculated.

The results in figure 1 demonstrate the influence of size asymmetry on the non-equilibrium structure $f(s)$. As seen, the entire function shifts to lower and lower values with increasing size asymmetry. Thus, shear perturbs the equilibrium structure less for pairs of unequal spheres than for equal-sized spheres. This then has a similar influence on the Brownian contribution to the Huggins coefficient, which is a weighted integral over this function. A similar reduction in the non-equilibrium structure has been reported for the sedimentation problem (for equal particle densities) by Batchelor & Wen (1982*b*).

Results for numerical integration of the functions $I^B(\lambda)$ and $I^H(\lambda)$ are shown in table 1 (these functions are defined so as to be equivalent upon $\lambda \rightarrow 1/\lambda$ substitution).

As discussed in more detail in Appendix A, we judge the relative error in the numerical calculation to be unacceptable for size ratios greater than 10, and hence, do not report results for larger size ratios. The results for $\lambda = 1$ compare well with previous calculations of Batchelor (1977) ($I^B(\lambda) = 0.97$ and $I^H(\lambda) = 2.7$) and the later, more precise calculations of Cichocki & Felderhof (1988) ($I^B(\lambda) = 0.913$ and $I^H(\lambda) = 2.5$),

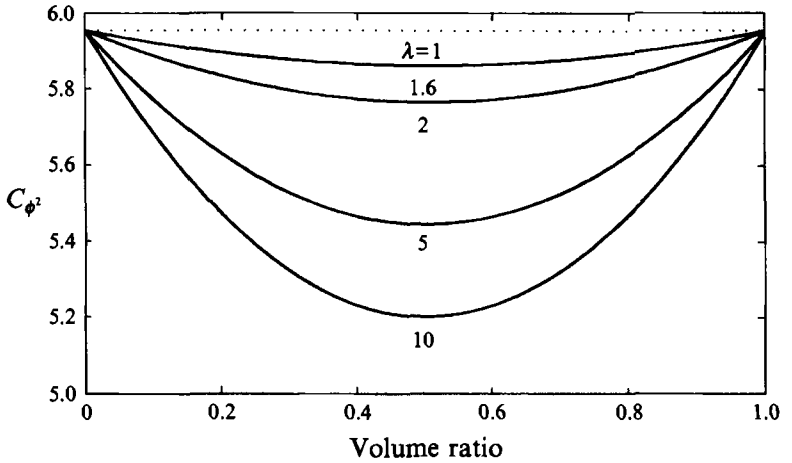

FIGURE 2. The ϕ^2 coefficient of viscosity ($k_H * 2.5^2$) for hard-spheres as a function of volume ratio for various degrees of size asymmetry, as labelled.

the primary difference being approximations involved in Batchelor's interpolations for the hydrodynamic functions, as also discussed by Kim & Mifflin (1985).

These results are plotted as C_{ϕ^2} coefficients ($C_{\phi^2} = k_H * 2.5^2$) as a function of mixing volume ratio $\phi_1/(\phi_1 + \phi_2)$ and size asymmetry (λ) in figure 2. As seen, the viscosity minimum deepens with increasing polydispersity and is symmetric in mixing volume ratio. Further, the magnitude of the effect is modest, as a significant fraction of the coefficient is independent of size ratio (the part coming from renormalization).

Experimental results for capillary viscometry on dilute suspensions of colloidal hard-sphere silica particles by Woutersen & de Kruif (1993) show some similarities and differences. For size asymmetries of 1.45 and 1.59, a reduction in the C_{ϕ^2} coefficient of similar magnitude to the predictions is seen upon mixing. Although the magnitude of the viscosity reduction with mixing is comparable within the measuring uncertainty, the experimental results are not as symmetric in mixing volume fraction, showing a slight skewedness toward the larger size. However, larger size asymmetries show an increase upon mixing, which is not consistent with the trends computed here for hard spheres. Woutersen & de Kruif (1993) speculate that this arises from interparticle forces due either to surface charges or depletion forces, neither of which is accounted for in this dilute limiting, hard-sphere theory. The latter possibility arises from three-body interactions even in very dilute suspensions, which if true suggests that accurate measurement of the Huggins coefficient for hard-sphere mixtures is virtually impossible. Although there are numerous studies demonstrating viscosity reductions for more concentrated systems, we are unaware of any other studies that examine the dilute limiting viscosity for hard-sphere colloidal suspensions that would be available for comparison.

The reason for the symmetry in the Huggins coefficient with volume ratio is evident from examination of the basic formulas for the stress dipoles. For example, the hydrodynamic stress dipole is given by an expression with the following form by Batchelor & Green (1972*a*, *b*) as

$$\boldsymbol{S}_{ij}^{H} = \frac{20}{3}\pi a_i^3 \mu_o \left[\mathrm{Re}(\boldsymbol{E}_{ij}, K'(\lambda), L'(\lambda), M'(\lambda), \mathbf{s}_{ij})\right], \tag{4.1}$$

with the functional dependence of Re indicated. So, the dissipation of a particle of type i in the presence of another particle j scales as the volume of particle of type i times a function of the size ratio, applied flow, and interparticle separation. The total dissipation, then, scales as the number of type i times the volume of this particle type, summed over all particle types. The symmetry of the dipole expression for $\lambda \rightarrow 1/\lambda$ inversion then yields the symmetry in the final viscosity (hydrodynamic contribution) for bimodal suspensions. A similar argument holds for the Brownian contribution to the total suspension viscosity. As shown by Batchelor (1977), the Brownian contribution to the stress can be written as

$$\frac{-1}{V}\sum_i \boldsymbol{U}_i \boldsymbol{F}_i^B, \tag{4.2}$$

where

$$\boldsymbol{U}_i = \boldsymbol{E}\cdot\boldsymbol{R}_i + \mathbf{E}:\boldsymbol{C}_i.$$

By symmetry of forces, the leading term is necessarily zero in the summation, while the interaction term, as characterized by the hydrodynamic tensor $\boldsymbol{C}$, is proportional to the stress dipole discussed above. Therefore, the Brownian stress has the same symmetry in volume fraction as the hydrodynamic stress contribution, leading to the same symmetry in the Huggins coefficient with volume ratio.

In the experimental studies a viscosity reduction upon mixing is most often observed for bimodal suspensions. However, the viscosity minimum is usually seen to lie toward suspensions rich in particles of the large size when plotted against volume ratio. A similar result has been seen in an approximate calculation by van Iersel (1987) which included many-body thermodynamic forces. A more complicated asymmetry was obtained by Ohtsuki (1983) for spheres with both size and charge asymmetry. Thus, the presence of asymmetry can be attributed to particle interactions beyond the pair level and asymmetry in the pair interaction potential.

Some hypotheses for the reduction in viscosity upon mixing two different sizes of particles have invoked an excluded-volume argument (Sweeny & Geckler 1954; Chong *et al.* 1971; Ackermann & Shen 1979; Goto & Kuno 1984; Shapiro & Probstein 1992). Size asymmetry results in a lower total excluded volume for the same overall volume fraction. This reduction in excluded volume is thought to decrease the viscosity primarily by increasing the maximum packing fraction and the free volume in the suspension. It is unclear if this argument applies to dilute suspensions; however, the equations derived for high volume fractions will indeed predict a viscosity reduction at lower volume fractions.

An alternative and perhaps more mechanistic explanation is suggested by the calculations presented here for dilute suspensions. As seen, the hydrodynamic coefficients that give the dissipation of energy for two spheres in a flow field are lowered by the presence of size asymmetry with respect to the equal-size limit. This effect dominates in the near field. A calculation using the far-field forms of the hydrodynamic functions (which neglect all near field lubrication forces) yields the exact opposite effect (see Appendix B). Thus, as seen in the plots of the function $\hat{J}(s,\lambda)$ in Appendix A, the dissipation due to the applied flow is greatly reduced for spheres in the near field of the hydrodynamic interaction range. This shows that the smaller particles are *shielded* by the larger from the applied flow field when they are in close proximity. A similar phenomenon has been reported by Batchelor & Wen (1982*b*) for sedimentation in a polydisperse suspension where the smaller particle follows in the wake of the larger, and consequently, also for collective diffusion (Batchelor 1983*a*). As the hydrodynamic

coupling is important in driving the non-equilibrium structure and directly determines the stresslet due to Brownian motion, the Brownian contribution also decreases with increasing size asymmetry because of this shielding. This can be seen quantitatively in figure 1 and in the plot of the $W(s,\lambda)$ hydrodynamic function in Appendix A. One expects this phenomenon also to be of relevance at higher concentrations, where particles are forced into the near field due to packing constraints.

4.2. *Polydisperse Huggins coefficient*

The above results for bimodal suspensions can be used to directly calculate the Huggins coefficient for suspensions of polydisperse spheres if the size distribution is known. For the purpose of illustration, we will assume a simple Schulz size distribution as a realistic model for the polydispersity and use this to calculate the variation in the Huggins coefficient with polydispersity index. This calculation will be used to access the influence of polydispersity on viscosity measurements in the dilute limit.

A commonly used model for a particle size distribution that is continuous and normalized is the Schulz distribution (see Mittelbach 1965; van Beurten & Vrij 1981; Hayter 1985). This distribution has the necessary qualities that it does not have negative values for radii and that it decays sufficiently rapidly for both large and small size ratios to yield a physically meaningful distribution (Wagner *et al.* 1991). Defining $\rho(a)$ as the normalized probability of occurrence of particles of radius a results in

$$\rho(a) = (z+1)^{z+1}x^z \frac{\exp^{-(z+1)x}}{\bar{a}\Gamma(z+1)}, \tag{4.3}$$

where $\bar{a}$ is the mean particle size and $x = a/\bar{a}$, $z = (1-t^2)/t^2$, $t = \sigma/\bar{a}$ with σ^2 the variance, Γ the gamma function, and $z_j = z + j$. Another convenient property of the Schulz distribution is the ability to express the ratio of any of the size moments in terms of readily calculable functions of the polydispersity:

$$X_n = \frac{\langle a^n \rangle}{\langle a \rangle^n} = \frac{\prod_{j=2}^{n} z_j}{z_1^{n-1}}. \tag{4.4}$$

Again, there are other possible distributions that could be used in place of the Schulz distribution; we are using this one, however, to provide a simple method of determining how polydispersity can influence the Huggins coefficient. Typical results for this distribution are shown in figure 3, where the distributions are scaled to have the same maximum value to emphasize the effects of the variance.

The general formula for the stress to the ϕ^2 level for a polydisperse suspension is written as

$$\frac{\eta}{\mu_o} = 1 + \frac{5}{2}\phi + \phi^2\left(\frac{5}{2} + \frac{1}{v^2}\int_0^\infty \int_0^\infty I(\lambda)\frac{4\pi a^3}{3}\frac{4\pi b^3}{3}\rho(a)\rho(b)\mathrm{d}a\mathrm{d}b\right), \tag{4.5}$$

where the function $I(\lambda) = I^H(\lambda) + I^B(\lambda)$ has been defined above. The function v is just the average volume per particle, which upon substitution for the Schulz distribution for $\rho(a)$ yields

$$v = \frac{4\pi\langle a^3 \rangle}{3} = \frac{4\pi\langle a \rangle^3}{3} X_3. \tag{4.6}$$

To proceed further, a numerical calculation is required as there is no analytic form for the function $I(\lambda)$. Unfortunately this procedure, although formally possible,

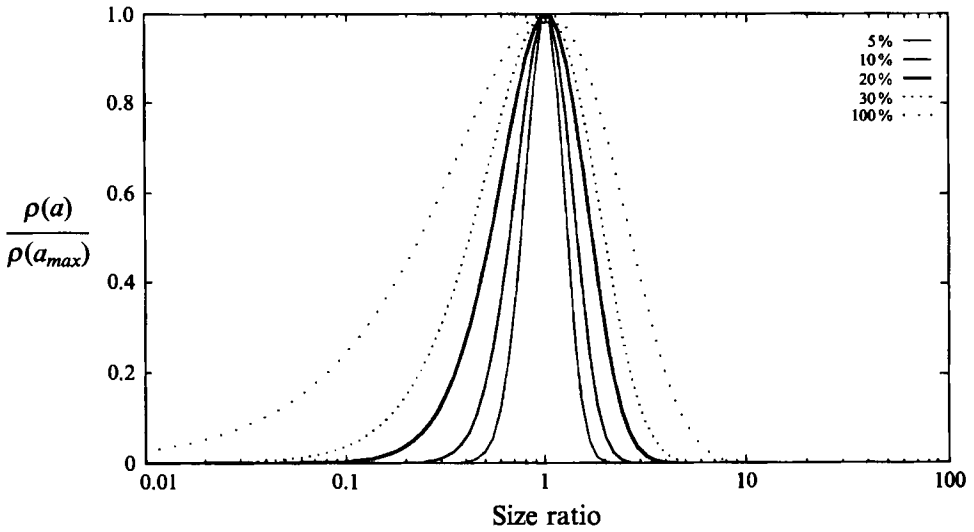

FIGURE 3. Schulz distribution, normalized, as a function of polydispersity, as labelled.

is computationally intractable due to the extremely time-consuming computations required to construct the function $I(\lambda)$ at sufficiently fine grid points. Hence, we have taken another tack whereby the appropriate value for $I(\lambda)$ is determined by an analytic interpolation formula. Although a simple cubic spline fit to the numerical data is possible, we propose an interpolation formula based on physical insight. This parameterization helps in reducing the integral to one dimension and should be sufficiently accurate for our purposes here.

The function $I(\lambda)$ has the symmetry property $I(\lambda) = I(1/\lambda)$ and must smoothly asymptote to constant values as $\lambda \to \infty$ and $\lambda \to 0$. Further, as discussed above, our numerical results are limited to size ratios below 10 (or above 0.1), based on the numerical accuracy of the calculated hydrodynamic functions. An analytical form that is capable of capturing these requirements is given by

$$I(\lambda) = (I(\lambda = 1) - I(\lambda \to \infty))\, \mathrm{e}^{-\beta[(1-\lambda^2)/\lambda]} + I(\lambda \to \infty). \tag{4.7}$$

Because of the limitations on the hydrodynamic coefficients, we choose $I(\lambda \to \infty) = I(\lambda = 10)$. The data for I^H and I^B were fit independently to the above relationship, as shown in figure 4, with values of the derived coefficient β of 0.583 and 0.4811 respectively. As shown, the analytical fits are in reasonable agreement. This approximation is justified from close examination of the Schulz distribution plot, figure 3. Even for 100% polydispersity, a negligibly small fraction of the particle sizes lies outside the interval $0.1 < \lambda < 10$. Thus, it is more relevant to accurately represent the functions within this interval, especially since the contributions from highly asymmetric particle size ratios are also weighted less.

The two-dimensional integral in (4.5) can be reduced to a one-dimensional integral through the variable substitution $b = a\lambda$. Direct substitution results in the following for the integral term:

$$\left(\frac{4\pi}{3v}\right)^2 \int_0^\infty \int_0^\infty I(\lambda)\lambda^3 a^6 \rho(a\lambda)\rho(a)\mathrm{d}\lambda\mathrm{d}a. \tag{4.8}$$

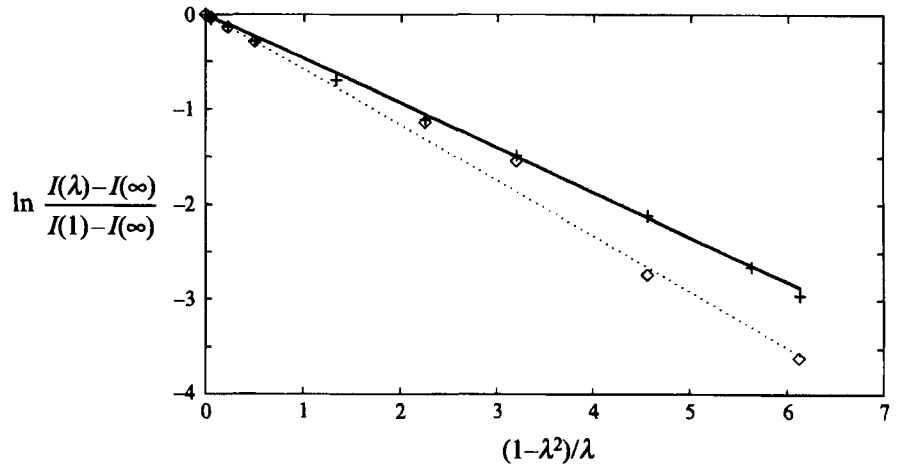

FIGURE 4. The functional fit to (4.7) for the Brownian contribution (—), data (+) and the hydrodynamic contribution (···), data (◇).

Substitution of the explicit formulas for the Schulz distributions and integration results in,

$$I(\lambda \to \infty) + \frac{\Gamma(2z+8)}{\Gamma(z+4)\Gamma(z+4)}(I(\lambda=1) - I(\lambda \to \infty)) \int_0^\infty e^{-\beta\frac{(1-\lambda)^2}{\lambda}} \frac{\lambda^{z+3}}{(1+\lambda)^{2z+8}} d\lambda. \quad (4.9)$$

This formula can be integrated for each force, Brownian and hydrodynamic, to yield the ϕ^2 coefficient for the polydisperse sample as a function of the normalized standard deviation s (the normalized square root of the variance).

Results for the integrations are shown in figure 5, where it is evident that the Brownian contribution is more sensitive to the polydispersity than the hydrodynamic and that the total effect is relatively small. A semilog plot demonstrates how the total ϕ^2 coefficient varies with the standard deviation (figure 6). The line is a best fit of a third-order polynomial with the form $C_{\phi^2} = 6.00 - 0.648*s + 0.334*s^2 - 0.0586*s^3$. From this figure it is evident that the monodisperse suspension has the highest viscosity coefficient and that even 10% polydispersity does not have a distinguishable effect on the coefficient. Further, a very broad distribution of 100% yields only a 6% reduction in the coefficient (extensions to broader distributions are subject to our calculational limitations). One can conclude, therefore, that the effects of polydispersity on the dilute limiting viscosity are rather modest in comparison to the effects of interparticle forces (see for example Russel 1984).

The authors are most grateful to Professor D. Jeffrey for providing the necessary programs to recalculate his published resistivities for unequal spheres and to Professor S. Kim for also providing copies of his programs. Financial support for this program was through the National Science Foundation (CTS-9158164). The authors wish to thank Dr Kees de Kruif for enabling collaboration between the authors.

Note added in proof: A recent article by Professor R.B. Jones, to appear in *Physica* A also presents an independent calculation of the hydrodynamic contribution to the Huggins coefficient for bimodal suspensions; the results are in agreement with those

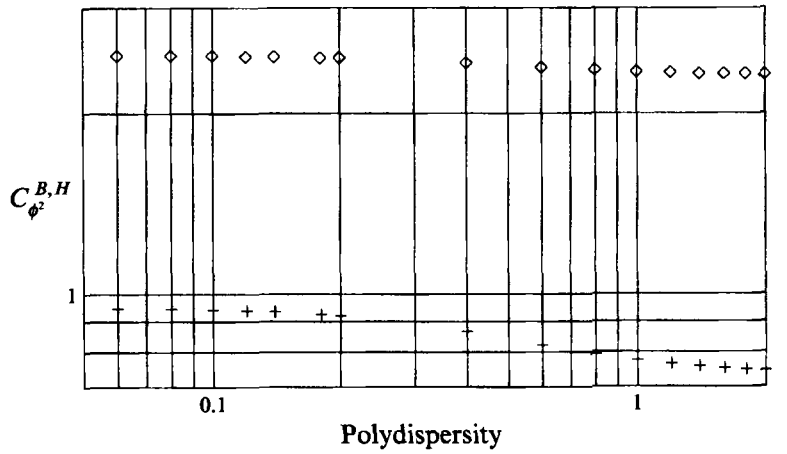

FIGURE 5. The C_{ϕ^2} coefficient for Brownian (+) and hydrodynamic (◇) forces as a function of polydispersity s.

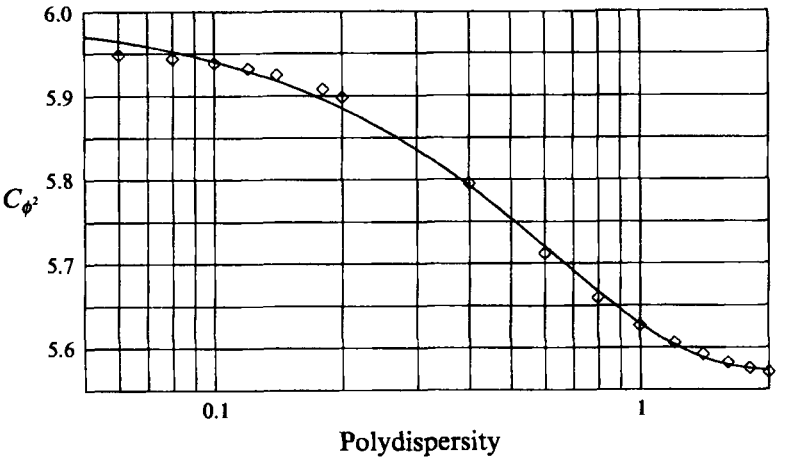

FIGURE 6. The total C_{ϕ^2} coefficient (◇). The curve (—) is a parametric fit, given by $k_H * 2.5^2 = 6.00 - 0.648 \bullet s + 0.334 * s^2 - 0.0586 * s^3$.

presented here. Further, Professor Jones presents an analytical value for $I^H(\lambda \to \infty)$ of 1.875, justifying our assumption in using equation (4.7).

Appendix A. Hydrodynamic functions

The relevant hydrodynamic functions required for the polydisperse calculations are derived from recently published results for unequal-sphere resistivities by Jeffrey (1992). A discussion of the physical meaning and source of these functions can be found in Russel *et al.* (1989) and Kim & Karrila (1991). The basic force, torque, stress relations to the applied velocity fields and particle velocities can be expressed either as mobilities, or the inverse, resistivities. The inverse relations for these functions can be found in Kim & Mifflin (1985), Jeffrey & Onishi (1984), and Kim & Karrila (1991), and so will not be reproduced here. Given the mobilities from

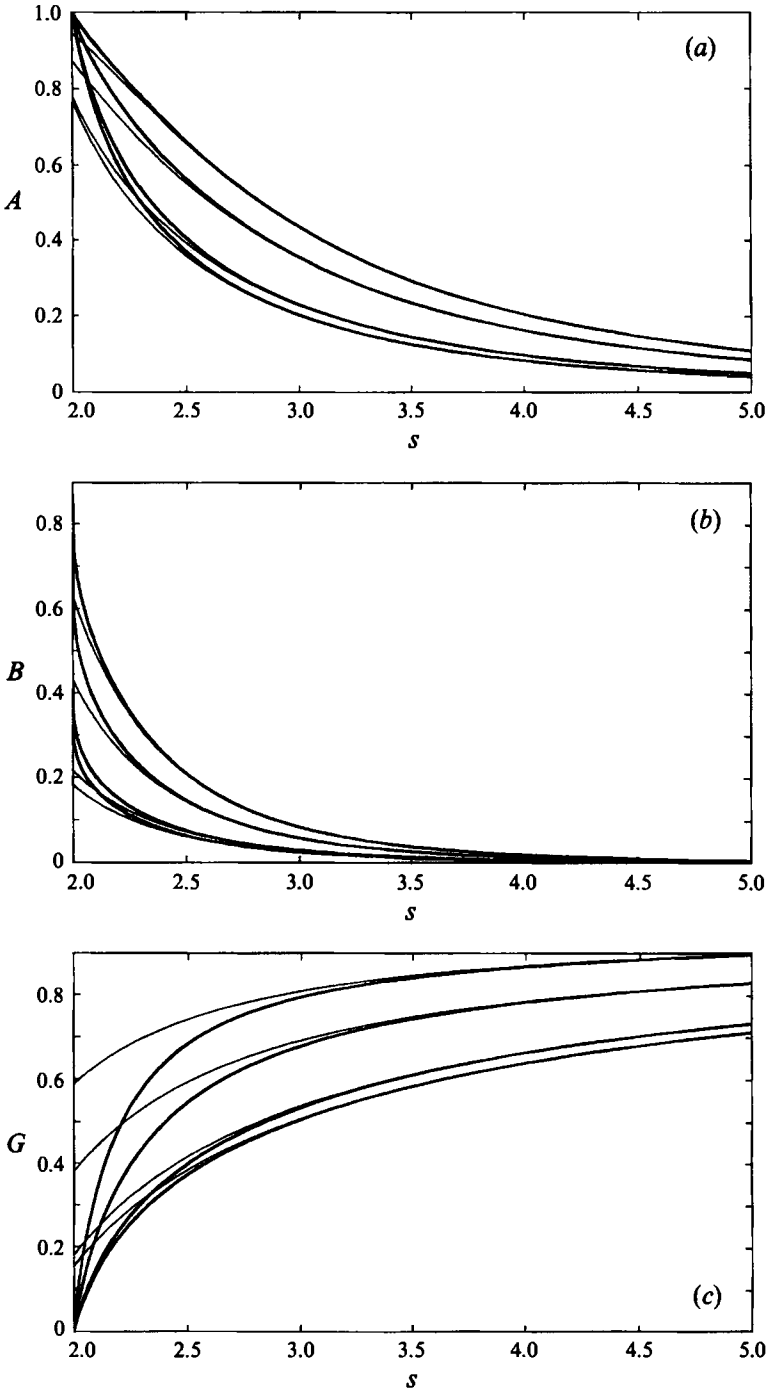

FIGURE 7(*a–c*). For caption see facing page.

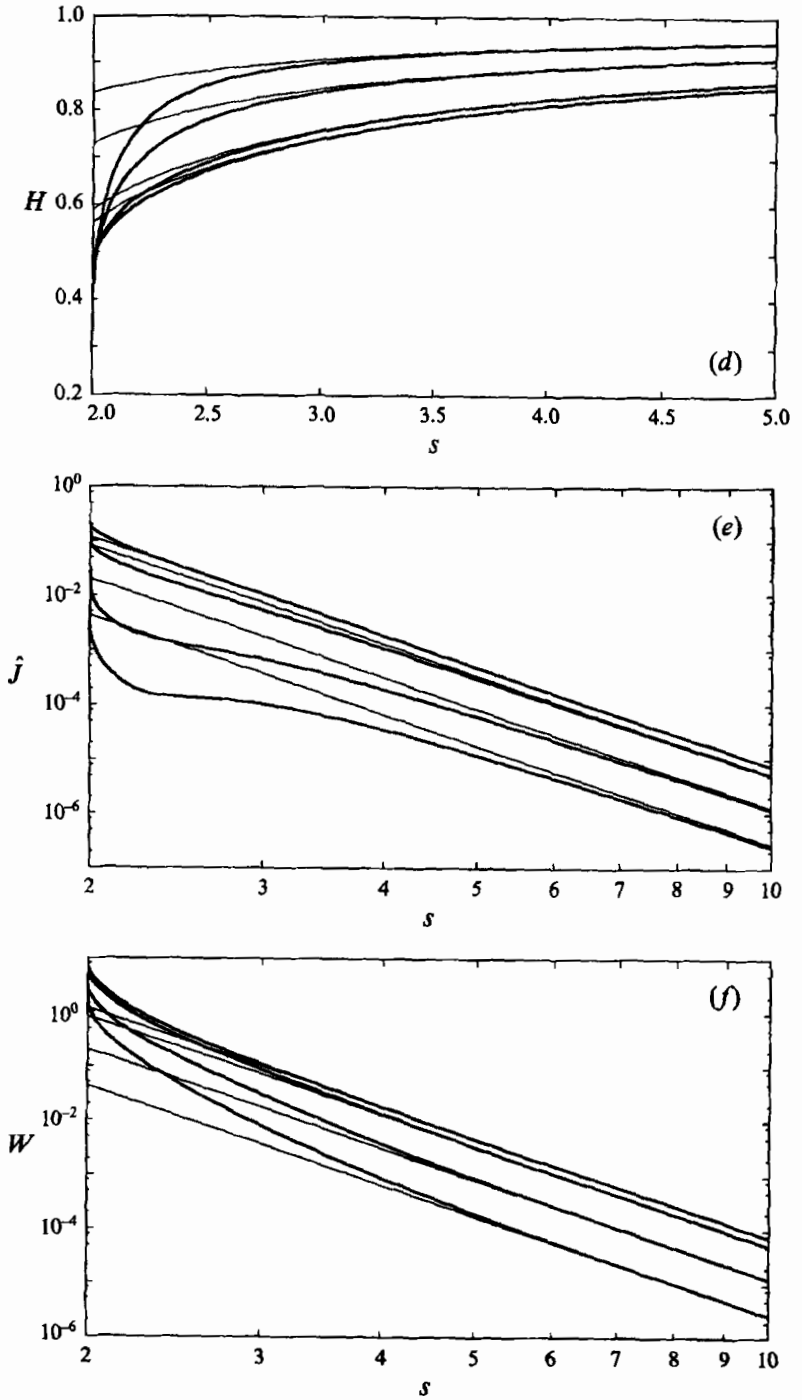

FIGURE 7. Hydrodynamic functions calculated for various values of size polydispersity (thick line), and the far-field form (thin line) for $\lambda = 10, 5, 2, 1$ from top to bottom, respectively. (*a*) $A(s,\lambda)$; (*b*) $B(s,\lambda)$; (*c*) $G(s,\lambda)$; (*d*) $H(s,\lambda)$; (*e*) $\hat{J}(s,\lambda)$; (*f*) $W(s,\lambda)$.

numerical inversion of the required resistance matrices, whose elements are available numerically from the work of Jeffrey (1992), the required hydrodynamic coefficients are then given as combinations:

$$A(s;\lambda) = \frac{2}{5}\left(\frac{2}{1+\lambda}\hat{x}^g_{11} - \hat{x}^g_{12} + \hat{x}^g_{21} - \frac{2\lambda}{1+\lambda}\hat{x}^g_{22}\right), \tag{A 1}$$

$$B(s;\lambda) = \frac{4}{5}\left(\frac{2}{1+\lambda}\hat{y}^g_{11} - \hat{y}^g_{12} + \hat{y}^g_{21} - \frac{2\lambda}{1+\lambda}\hat{y}^g_{22}\right), \tag{A 2}$$

$$W(s;\lambda) = 3(A(s;\lambda) - B(s;\lambda)) - \frac{\mathrm{d}}{\mathrm{d}s}(A(s;\lambda)), \tag{A 3}$$

$$G(s;\lambda) = \frac{\lambda\hat{x}^a_{11} + \hat{x}^a_{22}}{1+\lambda} - \frac{4\lambda\hat{x}^a_{12}}{(1+\lambda)^2}, \tag{A 4}$$

$$H(s;\lambda) = \frac{\lambda\hat{y}^a_{11} + \hat{y}^a_{22}}{1+\lambda} - \frac{4\lambda\hat{y}^a_{12}}{(1+\lambda)^2}, \tag{A 5}$$

$$\hat{J}(s;\lambda) = \frac{\lambda^3 J(s;\lambda^{-1}) + J(s;\lambda)}{(1+\lambda^3)}, \tag{A 6}$$

$$J(s;\lambda) = -1 - \tfrac{1}{5}\left(\hat{x}^m_1 + 2\hat{y}^m_1 + 2\hat{z}^m_1\right), \tag{A 7}$$

$$\begin{aligned}\hat{x}^m_1 = &-\left(\hat{X}^M_{11} + \left(\frac{1+\lambda}{2}\right)^3\hat{X}^M_{12}\right) + \frac{4}{5}\hat{X}^G_{11}\left(\hat{x}^g_{11} + \frac{1+\lambda}{2}\hat{x}^g_{21}\right)\\ &+\frac{4}{5}\hat{X}^G_{12}\left(\left(\frac{1+\lambda}{2}\right)^3\hat{x}^g_{12} + \lambda\left(\frac{1+\lambda}{2}\right)^2\hat{x}^g_{22}\right),\end{aligned} \tag{A 8}$$

$$\begin{aligned}\hat{y}^m_1 = &-\left(\hat{Y}^M_{11} + \left(\frac{1+\lambda}{2}\right)^3\hat{Y}^M_{12}\right) + \frac{12}{5}\hat{Y}^G_{11}\left(\hat{y}^g_{11} + \frac{1+\lambda}{2}\hat{y}^g_{21}\right)\\ &+\frac{12}{5}\hat{Y}^G_{12}\left(\left(\frac{1+\lambda}{2}\right)^3\hat{y}^g_{12} + \lambda\left(\frac{1+\lambda}{2}\right)^2\hat{y}^g_{22}\right)\\ &+\frac{12}{5}\hat{Y}^H_{11}\left(\hat{y}^h_{11} + \hat{y}^h_{21}\right) + \frac{12}{5}\left(\frac{1+\lambda}{2}\right)^3\hat{Y}^H_{12}\left(\hat{y}^h_{12} + \hat{y}^h_{22}\right),\end{aligned} \tag{A 9}$$

$$\hat{z}^m_1 = -\left(\hat{Z}^M_{11} + \left(\frac{1+\lambda}{2}\right)^3\hat{Z}^M_{12}\right). \tag{A 10}$$

All coefficients with a carat are non-dimensional coefficients and follow the notation of Kim & Mifflin (1985).

Note that the final coefficients are symmetric upon λ inversion while many of the intermediate coefficients are not. These coefficients, as functions of s for various values of λ are shown numerically in figures 7 and 8. Because of the multiple levels of numerical calculation, it was imperative to check these against known, limiting values. All the functions were checked against the far-field forms, given below and shown in the plots:

$$A(s;\lambda) = \frac{20(1+\lambda^3)}{(1+\lambda)^3 s^3} - \frac{48(1+\lambda^5) + 80\lambda^2(1+\lambda)}{(1+\lambda)^5 s^5} + \ldots, \tag{A 11}$$

$$B(s;\lambda) = 32\frac{1+\lambda^5 + \frac{5}{3}\lambda^2(1+\lambda)}{(1+\lambda)^5 s^5} + \ldots, \tag{A 12}$$

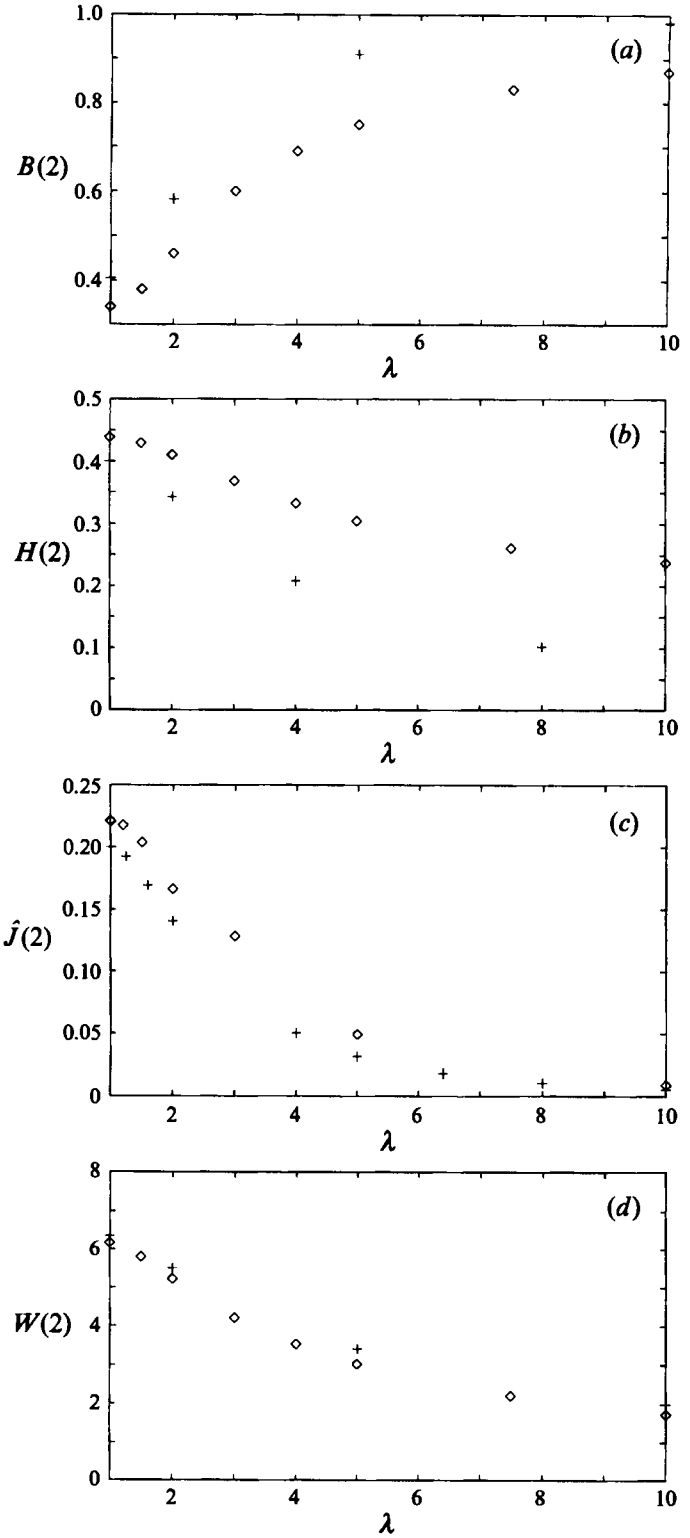

FIGURE 8. Comparison of contact values the hydrodynamic functions against published results. (*a*) $B(s = 2, \lambda)$ ($\diamond$) against the published results of Jeffrey (1992) (+). (*b*) $H(s = 2, \lambda)$ ($\diamond$) against the published results of Jeffrey & Onishi (1984) (+). (*c*) $\hat{J}(s = 2, \lambda)$ (+) against the published results of Nir & Acrivos (1973) ($\diamond$). (d) $W(s = 2, \lambda)$ ($\diamond$) against the results of Jeffrey (1992) (+).

$$G(s;\lambda) = 1 - \frac{3}{2}\frac{\alpha}{s} + \ldots, H(s;\lambda) = 1 - \frac{3}{4}\frac{\alpha}{s} + \ldots, \tag{A 13}$$

$$\hat{J}(s;\lambda) = \frac{15}{2}\alpha^3 s^{-6} + \ldots, W(s;\lambda) = 75\alpha^3 s^{-6} + \ldots, \tag{A 14}$$

$$\alpha = \frac{4\lambda}{(1+\lambda)^2}. \tag{A 15}$$

The numerical calculations all converged to the far-field forms, most by s values on the order of $s \leqslant 5$. The most notable deviation is seen for the function $\hat{J}$, where the far-field form is not valid until very large values of s for highly asymmetric size ratios. Limiting values at contact ($s = 2$) are also known for the functions B, H, and $\hat{J}$. As seen, these are also in reasonable agreement. It is important to note that the coefficients used here are inverted from Jeffrey's resistivities, which were calculated numerically from Jeffrey's programs using 200 term summations. Therefore, some level of numerical inaccuracy arises when large terms cancel at contact to yield the desired coefficient.

Appendix B. Far-field hydrodynamics approximation

As a check of the numerical accuracy of our calculations and as a possible indicator of the qualitative trends, we calculated the Huggins coefficient based upon the analytical use of far-field hydrodynamics. The approximation replaces the functions $\hat{J}$ and W by their first-order, far-field forms, as given in Appendix A above, in the stress expressions. The functions G and H are also set to 1, the leading-order term, in the Smoluchowski equation. Because of the far-field approximations the boundary condition at contact must be replaced by a no-flux condition:

$$G(s,\lambda)\frac{\mathrm{d}f(s,\lambda)}{\mathrm{d}s} + s(1 - A(s,\lambda)) = 0. \tag{B 1}$$

This then enables an analytic calculation of the non-equilibrium structure to leading order, as (see for example Russel *et al.* 1989):

$$f(s,\lambda) = \frac{32}{3}s^{-3} + \vartheta(s^{-4}). \tag{B 2}$$

It is to be noted that the leading-order term is independent of the size ratio, which is a consequence of neglecting the important lubrication forces in the contact boundary condition. Thus, this is not the correct far-field form for the full solution. Using this and the analytical expressions for the hydrodynamic coefficients $\hat{J}$ and W leads to the following expressions for the integrals:

$$I^H(\lambda) = \frac{75}{8}\frac{1+\lambda^3}{(1+\lambda)^3}, \; I^B(\lambda) = \frac{15}{8}\frac{\lambda}{(1+\lambda)^2}. \tag{B 3}$$

Thus, the total Huggins coefficient becomes:

$$K_H = \frac{2}{5} + \frac{9}{20}\frac{(\phi_1^2+\phi_2^2)}{\phi^2} + \frac{3}{(1+\lambda)^3}\frac{\phi_1\phi_2}{\phi^2}\left(1+\lambda^3+\frac{\lambda}{5}(1+\lambda)\right). \tag{B 4}$$

This is plotted as the ϕ^2 coefficient in figure 9, where it is seen that the far-field approximation has the same general symmetry as the exact numerical calculations. However, in the far-field approximation the Huggins coefficient actually *increases* with size inequality, the opposite trend to that in the exact calculation. This comparison

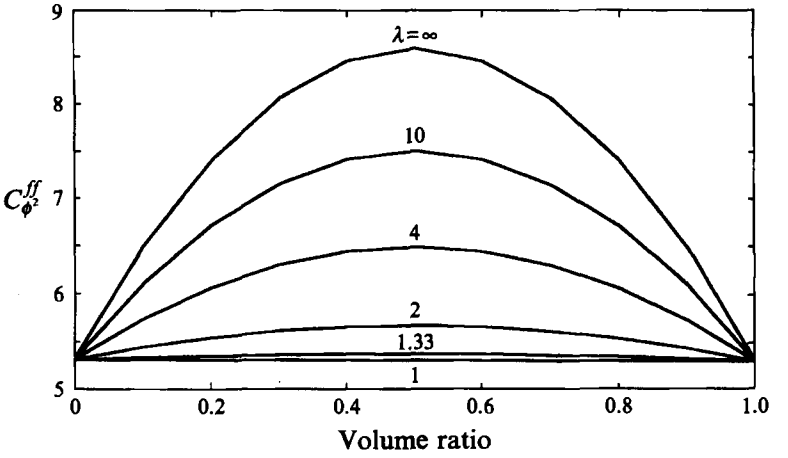

FIGURE 9. The $C^{ff}_{\phi^2}$ coefficient in the far-field hydrodynamic approximation for various size ratios λ as a function of mixing volume ratio.

supports the interpretation that the near-field hydrodynamic shielding occurs and is important in determining both the non-equilibrium structure and the stress dipoles.

REFERENCES

ACKERMANN, N. L. & SHEN, H. T. 1979 Rheological characteristics of solid-liquid mixtures. *AIChE J.* **25**, 327–332.

BATCHELOR, G. K. 1976 Brownian diffusion of particles with hydrodynamic interaction. *J. Fluid Mech.* **74**, 1–29.

BATCHELOR, G. K. 1977 The effect of Brownian motion on the bulk stress in a suspension of spherical particles. *J. Fluid Mech.* **83**, 97–117.

BATCHELOR, G. K. 1983 Diffusion in a dilute polydisperse system of interacting spheres. *J. Fluid Mech.* **131**, 155–175 and Corrigendum. **137**, 467–469.

BATCHELOR, G. K. & GREEN, J. T. 1972*a* The hydrodynamic interaction of two small freely-moving spheres in a linear flow field. *J. Fluid Mech.* **56**, 375–400.

BATCHELOR, G.K. & GREEN, J.T. 1972*b* The determination of the bulk stress in a suspension of spherical particles to order c^2. *J. Fluid Mech.* **56**, 401–427.

BATCHELOR, G. K. & WEN, C.-S. 1982*a* Sedimentation in a dilute polydisperse system of interacting spheres. Part 1. General theory. *J. Fluid Mech.* **119**, 379–408.

BATCHELOR, G. K. & WEN, C.-S. 1982*b* Sedimentation in a dilute polydisperse system of interacting spheres. Part 2. Numerical results. *J. Fluid Mech.* **124**, 495–528.

BRADY, J. F. 1993*a* The rheological behavior of concentrated colloidal suspensions. *J. Chem. Phys.* **99**, 567–581.

BRADY, J. F. 1993*b* Brownian motion, hydrodynamics, and the osmotic pressure. *J. Chem. Phys.* **98**, 3335–3341.

BRADY, J. F. & BOSSIS, G. 1988 Stokesian dynamics *Ann. Rev. Fluid Mech.* **20**, 111–157.

CHANG, C. & POWELL, R. L. 1993 Dynamic simulation of bimodal suspensions of hydrodynamically interacting spherical particles. *J. Fluid Mech.* **253**, 1–25.

CHONG, J. S., CHRISTIANSEN, E. D. & BAER, A. D. 1971 Rheology of concentrated dispersions. *J. Appl. Poly. Sci.* **15**, 2007–2021.

CICHOCKI, B. & FELDERHOF, B. U. 1988 Long-time self-diffusion coefficient and zero-frequency viscosity of dilute suspensions of spherical Brownian particles. *J. Chem. Phys.* **89**, 3705–3709.

D'AGUANNO, B. & KLEIN, R 1991 Structural effects of polydispersity in charged colloidal dispersions. *J. Chem. Soc. Faraday Trans.* **87**, 379.

D'AGUANNO, B., KLEIN, R., MÉNDEZ-ALCARAZ, J. M., NAEGELE, G. 1993 Polydisperse complex fluids. In *Complex Fluids* (ed. L. Garrido). Springer.

DHONT, J. K. G. 1987 Steady state viscosity coefficients of charged colloidal systems. *Physica* A **146**, 541.

DHONT, J. K. G. 1989 On the distortion of the static structure factor of colloidal fluids under shear flow. *J. of Fluid Mech.* **204**, 421–431.

DICKINSON, E., PARKER, R., & LAL, M 1981 Polydispersity and the colloidal order-disorder transition. *Chem. Phys. Lett.* **79**, 578.

FARRIS, R. J. 1968 Prediction of the viscosity of multimodal suspensions from unimodal viscosity data. *Trans. Soc. Rheol.* **12**, 281–301.

FELDERHOF, B. U. 1988 The contribution of Brownian motion to the viscosity of suspensions of spherical particles. *Physica* A **147**, 203.

FELDERHOF, B. U. & JONES, R. B. 1987 Linear response theory of the viscosity of suspensions of spherical Brownian particles. *Physica* A **146**, 417.

GOTO, S. C. & KUNO, H. 1982 Flow of suspensions containing particles of two different sizes through a capillary tube. *J. Rheol.* **26**, 387–398.

GOTO, S. C. & KUNO, H. 1984 Flow of suspensions containing particles of two different sizes through a capillary tube. ii. effect of the particle size ratio. *J. Rheol.* **28**, 197–205.

HAYTER, J. B. 1985 Determination of the structure and dynamics of micellar solutions by neutron small-angle scattering. In *Physics of Amphiphiles: Micelles, Vesicles and Microemulsions* (ed. V. Degiorgio, & M. Corti), pp. 59–93. North-Holland.

HIEMENZ, P. 1986 *Principles of Colloid and Surface Chemistry*, 2nd edn. Marcel Dekker.

JEFFREY, D. J. 1992 The calculation of the low Reynolds number resistance functions for two unequal spheres. *Phys. Fluids* A **4**, 16–29.

JEFFREY, D. J. & ACRIVOS, A. 1976 The rheological properties of suspensions of rigid particles. *AIChE J.* **22**, 417.

JEFFREY, D. J. & ONISHI, Y. 1984 Calculation of the resistance and mobility functions for two unequal rigid spheres in low-Reynolds-number flow. *J. Fluid Mech.* **139**, 261–290.

JONES, R. B. & BURFIELD, G. S. 1982 Memory effects in the diffusion of an interacting polydisperse suspensions. *Physica* **111A**, 562.

KIM, S. & KARRILA, S. J. 1991 *Microhydrodynamics: Principles and Selected Applications*. Butterworth-Heinemann.

KIM, S. & MIFFLIN, R. T. 1985 The resistance and mobility functions of two equal spheres in low-Reynolds-number flow. *Phys. Fluids* **28**, 2033–2045.

MCQUARRIE, D. A. 1976 *Statistical Mechanics*. Harper and Row.

MITTELBACH, P. 1965 Einige spezielle bestimmungsmethoden von form und polydispersitaet kolloider teilchen in verduennter loesung mittels roentgenkleinwinkelstreuung. *Kolloid-Z. und Z. Polymers* **206**, 152–159.

NIR, A. & ACRIVOS, A. 1973 On the creeping motion of two arbitrary-sized touching spheres in a linear shear field. *J. Fluid Mech.* **59**, 209–223.

OHTSUKI, T. 1981 Dynamical properties of strongly interacting Brownian particles: I, dynamic shear viscosity. *Physica* **108A**, 441–458.

OHTSUKI, T. 1983 Dynamical properties of strongly interacting Brownian particles III. *Physica* **122A**, 212–230.

PRESS, W. H., FLANNERY, B. P., TEUKOLSKY, S. A. & VETTERLING, W. T. 1986 *Numerical Recipes*. Cambridge University Press.

RODRIGUEZ, B. E., KALER, E. W. & WOLFE, M. S. 1992 Binary mixtures of monodisperse latex dispersions. 2. Viscosity. *Langmuir* **8**, 2382.

ROSCOE, R. 1952 The viscosity of suspensions of rigid spheres. *Brit. J. Appl. Phys.* **3**, 267–269.

RUSSEL, W. B. 1984 The Huggins coefficient as a means for characterizing suspended particles. *J. Chem. Soc. Faraday Trans.* (2) **80**, 31–41.

RUSSEL, W. B., SAVILLE, D. A. & SCHOWALTER, W. R. 1989 *Colloidal Dispersions*. Cambridge University Press.

SENQUN, M. Z., & PROBSTEIN, R. F. 1989 Bimodal model of slurry viscosity with application to coal-slurries. part 1. theory and experiment. *Rheol. Acta* **28**, 382–393.

SHAPIRO, A. P. & PROBSTEIN, R. F. 1992 Random packings of spheres and fluidity limits of monodisperse and bidisperse suspensions. *Phys. Rev. Lett.* **68**, 1422–1424.

STAPLETON, M. R., TILDESLEY, D. J., & QUIRKE, N. 1990 Phase equilibria in polydispere fluids. *J. Chem. Phys.* 7, 4456–4467.

SWEENY, K. & GECKLER, R. 1954 The rheology of suspensions. *J. Appl. Phys.* **25**, 1135–1144.

VAN BEURTEN, P. & VRIJ, A. 1981 Polydispersity effects in the small-angle light scattering of concentrated solutions of colloidal spheres. *J. Chem. Physics* **74**, 2744.

VAN IERSEL, M. W. F. 1987 *Viscosity of Bimodal Hard Sphere Suspensions.* Masters thesis, Princeton University.

WAGNER, N. J., KRAUSE, R., RENNIE, A. R., D'AGUANNO, B. & GOODWIN, J. 1991 The microstructure of charged, polydisperse colloidal suspensions by light and neutrons scattering. *J. Chem. Phys.* **95**, 494–508.

WAGNER, N. J., & RUSSEL, W. B. 1989 Nonequilibrium statistical mechanics of concentrated colloidal dispersions: Hard spheres in weak flows with many-body thermodynamics. *Physica* **155A**, 475–518.

WOUTERSEN, A. T. J. M. 1992 The rheology of adhesive hard sphere dispersions. PhD thesis, Utrecht.

WOUTERSEN, A. T. J. M. & DE KRUIF, C. G. 1993 The viscosity of semi-dilute bidisperse suspensions of hard spheres. *J. Rheol.* **37**, 681.